ments of the same group were about 50% high due to this source of error. The new σ_{H^+} values of Il'in *et al.*[19] agree well with our σ_{H^+} determinations[13] above 30 keV but fall drastically below our values at lower energies. As suggested by the authors,[19] errors in the low-energy data were perhaps caused by interception of large-angle dissociation fragments at the collision-chamber exit aperture; however, insufficient data on the collision chamber and detector geometry was given to allow us to confirm this.

Irsa and Friedman[20] concluded from mass spectrometer studies of H^+ and D^+ dissociation fragments of 4-keV HD^+ ions that the H^+ and D^+ fragments had mean transverse velocities of the order of 0.0024 times the HD^+ velocity. This result is not consistent with the present result assuming that the HD^+ ions of the earlier experiment possessed a dP/dR distribution similar to that of the H_2^+ ions used in the present experiment. Such an assumption leads to nearly an order-of-magnitude-larger angular spread than that observed by Irsa and Friedman.

[20] A. P. Irsa and L. Friedman, J. Chem. Phys. **34**, 330 (1961).

ACKNOWLEDGMENTS

The author is indebted to D. L. Allensworth for taking the experimental data, to J. M. Peek for calculating $\sigma(R,\varphi)$, and to J. M. Peek and T. A. Green for many stimulating discussions concerning the mechanism of collisional dissociation.

PHYSICAL REVIEW VOLUME 140, NUMBER 3A 1 NOVEMBER 1965

Dissociative Recombination in Neon: Spectral Line-Shape Studies*

T. Robert Connor† and Manfred A. Biondi
Department of Physics, University of Pittsburgh, Pittsburgh, Pennsylvania
(Received 1 June 1965)

Optical interferometric, spectrographic, and microwave techniques have been used to investigate the nature of electron-ion recombination in neon afterglows. Electron-density decay measurements yield a two-body recombination coefficient $\alpha \simeq 2\times10^{-7}$ cm³/sec, in agreement with earlier studies carried out at electron densities an order of magnitude smaller. The hypothesis that dissociative recombination, $Ne_2^+ + e \rightleftarrows (Ne_2^*)_{\text{unstable}} \rightleftarrows Ne^* + Ne +$ kinetic energy, is the process operative is tested by seeking to detect the kinetic energy of dissociation in the excited atoms produced by recombination. Fabry-Perot interferometer studies of the width of the λ5852 ($2p_1$-$1s_2$) neon line indicate that in the afterglow the line is very much broader than the thermal (300°K) atom width observed in the discharge. This excess width in the afterglow line is found to decrease with increasing neon gas pressure, owing to increased likelihood of excitation transfer from the fast atoms to thermal atoms before radiation. Higher-resolution studies of the spectral-line profiles indicate that the afterglow line consists of a "broad-shouldered," flat-topped component of the form expected for radiation from dissociatively produced excited atoms, surmounted by a narrow, thermal core resulting from radiation from slow-excited atoms produced by excitation transfer. The width of the fast-atom component of the profile yields a value for the dissociation kinetic energy, $E_D \simeq 1.2$ eV, leading to a binding energy for the neon molecular ion, $D(Ne_2^+) \simeq 1.4$ eV. The variation with neon pressure of slow-atom to fast-atom component in the line profile yields an excitation transfer cross section between excited $2p_1$ atoms and normal atoms of $Q_x \simeq (8\pm2)\times10^{-16}$ cm² at a relative velocity of 2.5×10^5 cm/sec. It is concluded that dissociative recombination is definitely the process responsible for the large electron loss in neon afterglows.

I. INTRODUCTION

THE present paper describes investigations designed to provide a critical test of whether or not dissociative recombination is the process responsible for the large electron loss rate observed in neon afterglows. The process of dissociative recombination was first suggested to account for the very large electron removal rates noted in ionospheric regions such as the E layer.[1] When microwave studies of noble-gas afterglows[2] gave evidence for large 2-body electron-ion recombination ($\alpha > 10^{-7}$ cm³/sec), dissociative recombination was proposed as the mechanism responsible.[3] For the case of neon, the process may be illustrated with the aid of Fig. 1 and the following equation,

$$Ne_2^+ + e \leftrightharpoons (Ne_2^*)_{\text{unstable}} \leftrightharpoons Ne^* + Ne + \text{kinetic energy}, \quad (1)$$

where the superscripts + and * indicate ionized and excited states, respectively. Thus, a molecular neon

* This research has been supported, in part, by the U. S. Office of Naval Research.

† Present address: Los Alamos Scientific Laboratories, Los Alamos, New Mexico.

[1] D. R. Bates and H. S. W. Massey, Proc. Roy. Soc. (London) **A187**, 261 (1964); **A192**, 1 (1947).

[2] M. A. Biondi and S. C. Brown, Phys. Rev. **76**, 1697 (1949).

[3] D. R. Bates, Phys. Rev. **77**, 718 (1950); **78**, 492 (1950); **82**, 103 (1951).

ion in a particular vibrational state captures an electron, without change of energy, to form an unstable excited state. (Such a transfer requires a favorable curve crossing of the type shown, so that there is appreciable overlap between the initial and final states.) The excited molecule begins to dissociate, and, if the internuclear separation increases beyond point X, it is no longer energetically possible for the electron to be released by autoionization, i.e., the first half of reaction (1) going to the left. The dissociation then proceeds to completion, producing two neon atoms, one probably in an excited state, moving apart with kinetic energies totalling E_D, the change of potential energy in the reaction. Since the time required for the atoms to separate many angstroms is of the order of 10^{-13} sec, the unstable excited molecule (radiative lifetime $>10^{-9}$ sec) has negligible chance of radiating, so that the reaction produces an excited *atom* (and thus atomic *line* radiation).

The dissociative process provides a mechanism potentially much more efficient than radiative capture of the electron, if the necessary curve crossings occur. Thus, qualitative theoretical arguments[3-5] have been advanced to support a two-body recombination coefficient, α_{diss}, of the order of 10^{-7} cm^3/sec or larger for thermal ($\sim$300°K) particles, in contrast to a radiative recombination coefficient $\alpha_{\text{rad}}<10^{-11}$ cm^3/sec at the same energy.[6] Quantitative theoretical calculations have not been carried out, since the details of the potential curves and their crossings, as well as the autoionization probability, depend on the wave functions for the various states involved, and these are not at present available.

The present experiment was undertaken to test the dissociative-recombination hypothesis by determining whether the atoms formed during recombination have kinetic energies substantially in excess of thermal energy (refer to Fig. 1). Previously,[7] experiments had shown that the large two-body recombination loss of electrons in argon occurred only when Ar_2^+ ions were expected to predominate. More recently, combined mass-spectrometer and microwave studies[8] of neon afterglows have shown that Ne_2^+ is the only significant afterglow ion when two-body recombination controls the electron loss.

Attempts to detect the kinetic energy of dissociation of the excited atoms formed by recombination in helium afterglows met with limited success.[9] In helium, circumstances are rather unfavorable for the detection of dissociative recombination, since, relative to the other

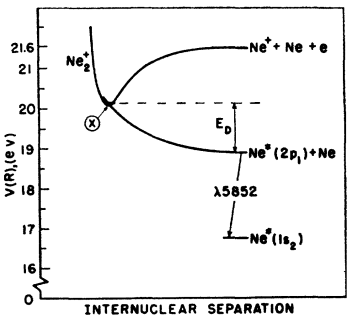

FIG. 1. Schematic representation of the potential energy $V(R)$ between two neon atoms as a function of their internuclear separation. Only two of the many curves are shown, one for the stable state of the molecular ion, Ne_2^+, the other for an unstable state of the excited molecule, Ne_2^*.

noble gases (e.g., neon and argon), the ambipolar diffusion loss rate is large and the dissociative-recombination coefficient is small ($<10^{-8}$ cm^3/sec). In addition, unlike neon and argon, the afterglow recombination spectrum shifts from predominantly atomic lines at low pressures ($\sim$1 Torr) to molecular bands at moderate pressures ($\gtrsim$10 Torr), suggesting a change in the recombination mechanism. The situation is further complicated by the fact that the 3-body process of collisional-radiative recombination[10] is not negligible compared to the expected dissociative recombination at the maximum electron densities used in the studies. (For $n_e\sim10^{10}$ e/cm^3, the equivalent coefficient for collisional-radiative recombination is predicted[10] to be "α"$_{\text{c.r.}}\sim10^{-9}$ cm^3/sec.) In fact, many of the observations of radiation emitted from flowing helium afterglows[11,12] are consistent with collisional-radiative recombination of both atomic and molecular helium ions with electrons, although other, detailed studies of microwave afterglows[13] indicate that some additional recombination mechanism is operative insofar as the helium molecular ions are concerned. A further problem with helium is the recent prediction[14] that the necessary potential curve crossings for dissociative recombination of He_2^+ ions and electrons only occur for ions in vibrationally excited states.

Although the dissociative reaction, Eq. (1), produces atoms with excess kinetic energy, detection of this kinetic energy through a Doppler effect in the radiation emitted from the excited atom requires that certain stringent conditions (discussed in detail in Sec. III) be met. While excess kinetic energy was detected in the excited atoms produced by recombination in low-

[4] E. Bauer and T. Y. Wu, Can. J. Phys. **34**, 1436 (1956).
[5] J. J. Gibbons, Abstracts of Defense Atomic Support Agency Reaction Rate Conference, Boulder, Colorado, 1961 (unpublished).
[6] See, for example, H. S. W. Massey and E. H. S. Burhop, *Electronic and Ionic Impact Phenomena* (Oxford University Press, London, 1952).
[7] M. A. Biondi, Phys. Rev. **129**, 1181 (1963).
[8] W. H. Kasner (private communication). This work was carried out with the apparatus described by W. H. Kasner and M. A. Biondi, Phys. Rev. **137**, A317 (1965).
[9] W. A. Rogers and M. A. Biondi, Phys. Rev. **134**, A1215 (1964).
[10] N. D'Angelo, Phys. Rev. **121**, 505 (1961); E. Hinnov and J. G. Hirschberg, *ibid.* **125**, 795 (1962); D. R. Bates, A. E. Kingston, R. W. P. McWhirter, Proc. Roy. Soc. (London) **A267**, 297 (1962); **A270**, 155 (1962).
[11] C. B. Collins and W. W. Robertson, J. Chem. Phys. **40**, 701, 2202, 2208 (1964), and J. Chem. Phys. (to be published).
[12] E. E. Ferguson, F. C. Fehsenfeld, and A. L. Schmeltekop, Phys. Rev. **138**, A381 (1965).
[13] D. E. Kerr, C. S. Leffel, and M. N. Hirsch (to be published).
[14] R. S. Mulliken, Phys. Rev. **136**, A962 (1964).

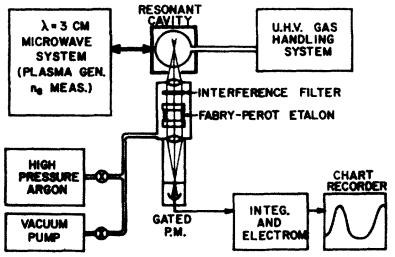

FIG. 2. Highly simplified block diagram of the experimental apparatus.

pressure helium afterglows, the results did not seem sufficiently conclusive to establish that dissociative recombination was definitely the origin of the radiation. We have, therefore, turned to neon, which had initially been regarded as less satisfactory in meeting the conditions for observation of the Doppler effect in the recombination radiation, in order to provide a test of the dissociative hypothesis in a case where the existence of a large, two-body recombination loss of electrons ($\alpha \simeq 2\times10^{-7}$ cm^3/sec) has been rather clearly established.[2,7,15]

The main aim of the experiment is to provide favorable circumstances for the detection of any excess kinetic energy of the excited atoms produced by recombination, resulting in limitations on the ranges over which other variables of interest, e.g., electron density and spectral line intensity, have been observed.

II. EXPERIMENTAL APPARATUS

The apparatus, shown rather schematically in Fig. 2, consists of four main parts; an ultrahigh-vacuum gas-handling system, a dual-mode microwave system to permit plasma generation and average electron density determinations during the afterglow, an optical spectrometer (not shown) to monitor the time history of the various radiations emitted during the afterglow, and a photoelectric recording Fabry-Perot interferometer to determine the widths and shapes of selected spectral lines in the afterglow. These components have been described in detail previously[9,16,17]; therefore only new features will be discussed in any detail here.

The gas handling vacuum system attains pressures between 10^{-9} and 10^{-8} Torr following bakeout of the main part of the system at $\sim$400°C. The quartz sphere, which during measurements is enclosed by the microwave cavity, is baked at $\sim$800°C. The pressure of the gas sample introduced into the sphere is measured by means of an oil manometer which is isolated from the gas-handling system by means of an ultrahigh vacuum null pressure detecting device. Airco reagent grade neon, contained in 1-liter glass flasks, is used in these studies.

Power from a high-power 3-cm cw magnetron generates a pulsed discharge lasting a few hundred microseconds and is repeated at either a 500-cps or a 286-cps rate. The magnetron operates through a ferrite isolator in a wave guide which is iris coupled into one mode of a rectangular parellelopiped resonant cavity. In the early studies a TE_{101}-mode cavity was used; in the later work, a larger, TE_{303}-mode cavity was employed. In each case, the largest practicable quartz sphere was placed within the cavity, one of radius 0.6 cm, the other 2.1 cm in radius.

A low-level 3-cm-wavelength probing signal excites a second mode of the cavity (the electric vector is perpendicular to that from the magnetron). Observations of the reflection of this signal are used to determine the cavity's resonant frequency and hence the average electron density as a function of time during the afterglow.[16] Use of the two orthogonal cavity modes reduces leakage of the high-power magnetron pulse into the probing signal guide to negligible proportions; therefore it has been possible to eliminate the nonoverloading amplifiers previously required.[9]

The radiation emitted in the discharge and during the afterglow is monitored by means of a Bausch and Lomb model 33-86-25 grating monochromator, using as a detector on RCA type-931A photomultiplier which is electronically gated "on" at selected times either in the discharge or the afterglow.

In order to obtain the width or shape of a given spectral line, that line is first isolated reasonably well from the rest of the spectrum by a narrow band ($\sim$17-Å half-width) Spectrolab interference filter and then passes through the photoelectric Fabry-Perot (F-P) interferometer[17] (see Fig. 2). The concentric rings of the F-P pattern are imaged by the output lens (f.l.=8 in.) on a plate containing a hole (0.0145 in. diam) which is aligned with the center of the pattern. In this way a small portion of the radiation in the central spot passes through and falls on the photocathode of a gated 931A photomultiplier. The multiplier's output signal is fed to an integrating circuit (time constant $\sim$4 sec) and electrometer whose output is displayed on the chart recorder.

The wavelength for constructive interference of the beams making up the center of the Fabry-Perot pattern is given by the relation

$$\lambda = 2\mu t/n, \qquad (2)$$

where λ is the vacuum wavelength, μ the refractive index of the medium between the plates, t the plate spacing, and n the interference order. This wavelength is made to change linearly with time by introducing argon gas at a constant rate to the sealed, initially evacuated housing containing the F-P plates; thus the refractive index between the plates increases linearly with time. If, now, the chart paper is driven by a synchronous motor, a linear presentation of intensity versus frequency over the line profile is obtained; the

[15] H. J. Oskam and V. R. Mittelstadt, Phys. Rev. 132, 1445 (1963).
[16] M. A. Biondi, Rev. Sci. Instr. 22, 500 (1951).
[17] M. A. Biondi, Rev. Sci. Instr. 27, 36 (1956).

frequency scale is calibrated by tuning through several interference orders, since the pattern repeats itself after a wave number interval of $\Delta\tilde{\nu}=(2\mu t)^{-1}\simeq(2t)^{-1}$.

In the early phases of the work reported in this paper, Fabry-Perot plates flat to 1/25 wavelength and coated with multilayer dielectric films of ~90% reflectivity were employed. The resulting finesse (the ratio of the free spectral range, $\Delta\tilde{\nu}_{fs}$, between interference orders to the instrumental half-width) is ~10. Thus, in a typical case, where $\Delta\tilde{\nu}_{fs}=(2\mu t)^{-1}=0.50$ cm^{-1} (1.0 cm spacer) an instrumental half-width of 0.05 cm^{-1} is expected. The thermal Doppler width for the visible transitions from excited neon atoms at 300°K is of the same magnitude; therefore the line shapes observed with these plates contain a large contribution of instrumental origin.

In order to observe more of the details of the line shapes, our later studies have been carried out with improved F-P plates, flat to 1/100 wavelength and coated with dielectric films of ~97% reflectivity. The resulting finesse of 42 yields instrumental widths in the range 0.010–0.016 cm^{-1} with the various spacers employed. These instrumental widths are sufficiently small that the observed line profiles closely approximate those of the radiated lines.

III. RELEVANT ATOMIC-COLLISION PROCESSES

Under the conditions of the experiment it is expected that, during the magnetron pulse, the plasma is created by electron impact excitation and ionization of the normal atoms. Atomic Ne^+ ions are formed directly, while Ne_2^+ ions result from associative ionization[18] when highly excited neon atoms combine with normal atoms. No evidence for appreciable ionization resulting from metastable-metastable collisions[19] and persisting into the afterglow is noted. Conversion of Ne^+ to Ne_2^+ as a result of three-body collisions involving two normal atoms presumably occurs with a coefficient of $\gtrsim 10^{-31}$ cm^6/sec.[20]

The principal loss processes for the electrons and ions during the afterglow are two-body volume recombination between the electrons and the Ne_2^+ ions and ambipolar diffusion of the electrons and positive ions to the walls of the quartz sphere.[21] In order to obtain a reasonably accurate determination of the recombination coefficient, electron density decay measurements were made at high pressures (~70 Torr) to reduce ambipolar diffusion loss to a small value over an appreciable portion of the afterglow and to assure that Ne_2^+ was the only significant afterglow ion.[8] Under these circumstances the electron continuity equation is adequately approximated by

$$\partial n_e/\partial t\simeq-\alpha n_e n_+\simeq-\alpha n_e^2, \qquad (3)$$

where n_e and n_+ are the electron and molecular ion densities, respectively. They have been set equal to satisfy the quasineutrality requirement for a plasma. The solution, $1/n_e=1/n_e(0)+\alpha t$, indicates that a measure of the recombination coefficient may be obtained from the observed slope of the curve of reciprocal electron density versus time.

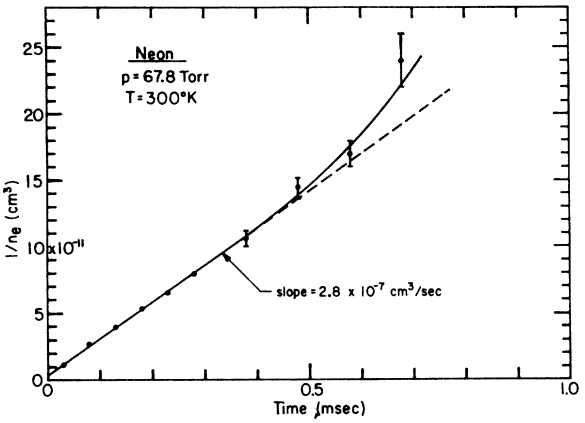

FIG. 3. Observed variation of the reciprocal of the electron density with time in a high-pressure neon afterglow.

An example of the decay of electron density observed with the TE_{101} mode cavity and small quartz sphere (fundamental-mode diffusion length, $\Lambda=0.19$ cm) is shown in Fig. 3. The electron decay follows the recombination law over a decade change in density and then departs in the direction expected for ambipolar diffusion contributions to the loss. The error bars show the uncertainties in the frequency determinations obtained with the cavity wavemeter. Following the convention of Gray and Kerr[22] the average electron-density values shown are obtained from the measured frequency-shift data on the unrealistic assumption of a uniform spatial distribution of electrons throughout the sphere. Then the slope of the curve, 2.8×10^{-7} cm^3/sec, is corrected for the effect of the actual electron spatial distribution expected,[22] yielding a recombination coefficient $\alpha=2\times10^{-7}$ cm^3/sec in excellent agreement with previous results.[2,7,15] An interesting feature of these measurements is that they refer to an electron density range ($\sim1-10\times10^{10}$ cm^{-3}) approximately an order of magnitude larger than that covered in the determinations of the earlier studies—indicating that the two-body recombination process predominates even in this higher density range.

The measured electron density decays with the TE_{303}-mode cavity and larger sphere also indicate recombination control of the afterglow at the pressures studied,

[18] J. A. Hornbeck and J. P. Molnar, Phys. Rev. **84**, 625 (1951).
[19] M. A. Biondi, Phys. Rev. **88**, 660 (1952).
[20] A. V. Phelps and S. C. Brown, Phys. Rev. **86**, 102 (1952); H. J. Oskam, Philips Res. Rept. **13**, 335, 401 (1958); E. C. Beaty and P. L. Patterson, Phys. Rev. **137**, A346 (1965).
[21] Under typical experimental conditions the effective coefficient for collisional radiative recombination (Ref. 10) is 10^{-8} cm^3/sec or less, more than an order of magnitude smaller than the two-body coefficient observed.
[22] E. P. Gray and D. E. Kerr, Ann. Phys. (N. Y.) **17**, 276 (1962).

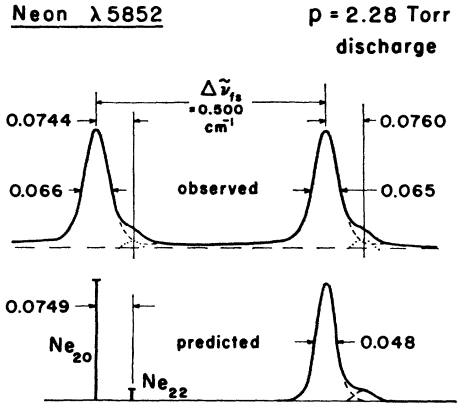

FIG. 4. Top: Observed neon λ5852 line shape during the microwave discharge at 300°K. The Fabry-Perot plates of finesse 42 were used for these observations. Bottom: Predicted isotope splitting and thermal Doppler-broadened shape in natural-abundance neon at 300°K.

20–74 Torr; however, conversion of the frequency shift data to absolute electron density values in the high-mode cavity is very uncertain. With the assumption (especially poor in this case) of a uniform spatial distribution of electrons in the sphere, the slopes of the $1/n_e$ versus t curves are found to be approximately 10^{-7} cm^3/sec, in qualitative agreement with the TE_{101}-mode cavity studies.

Although the electron density decay studies are carried out at high pressures to inhibit diffusion, the spectral line-shape studies require that measurements be carried out at rather lower pressures ($\sim 1-10$ Torr). This requirement stems from the fact that, even though the excited atoms formed during recombination may have excess kinetic energy, an associated Doppler effect will be noted in the radiation emitted only if the optical transition takes place both before the excited atom is slowed on collisions with normal atoms and before the excitation transfers from the fast-excited atom to a slow-normal atom. Since the rates of momentum transfer and excitation-transfer collisions vary linearly with the neon-atom concentration, a low gas pressure (and a short-excited-state lifetime) are necessary.

The λ5852 transition of neon ($2p_1 \rightarrow 1s_2$)[23] is a strong afterglow line with a reasonably short upper-state lifetime, $\tau = 1.5 \times 10^{-8}$ sec.[24] If momentum transfer between the fast-excited atoms and normal atoms occurs with a cross section in the range 10^{-16}–10^{-15} cm^2, then radiation will occur before the fast atom is slowed, provided that the pressure is less than ~ 10 Torr. A more serious obstacle is the possibility of excitation transfer to a slow-normal atom, since the cross section for such a process can be orders of magnitude larger than that for momentum transfer.[6] Here, it is not possible to guess in advance the magnitude of the process, but only to note that the spherical symmetry of the excited state[25] may make for a sufficiently weak interaction with the normal atom to yield the required small excitation transfer at pressures of $\gtrsim 1$ Torr.

IV. SPECTRAL LINE SHAPES

A. Isotope Effect

The λ5852 transition involves singlet states and therefore exhibits no fine structure; however, an isotope effect is noted in normal neon (90.8% Ne_{20} and 8.9% Ne_{22} abundance). The observed line shape during the discharge, using the F-P plates of finesse 42, is shown in the top half of Fig. 4. On the assumption that each isotope component is symmetrical about its central frequency, we have been able to decompose the trace into the two components, as indicated by the dashed and dotted lines. The observed hyperfine splitting of 0.075 ± 0.001 cm^{-1} is in excellent agreement with the theoretical value, 0.0749 ± 0.0005 cm^{-1}, calculated by Stone[26] and the value, 0.075 ± 0.003 cm^{-1}, measured by Nagaoka and Mishima.[27] In addition, the ratio of intensities of the components inferred from Fig. 4 is consistent with the natural isotopic abundance, although our determination is obviously not very accurate.

B. Thermal and Recoil Broadening

It is expected that, during the discharge, the λ5852 radiation is the result of electron impact excitation of normal neon atoms moving with ambient thermal speeds. The struck atom recoils slightly, adding this motion to the previous thermal speed. When the pressure is low, the atom will radiate before losing the recoil energy, and therefore a line slightly broader than the thermal Doppler width will be emitted. The shape of the line can be predicted by adaptation of an expression derived by Rogers and Biondi[9] for the case of dissociative broadening (see discussion in Sec. IV D).

In the microwave discharge, as a result of the rather small mean energy of the electrons (a few eV), most of the excitation of a given state results from electrons with kinetic energies near the threshold energy. From conservation of energy and momentum one finds that the recoil energy gained by a neon atom initially at rest is $E_R = (m/M)(E_x + 2\Delta E)$, where m and M are the electron and neon atom masses, respectively, E_x is the threshold excitation energy (~ 19 eV for the $2p_1$ state) and ΔE is the energy of the electron after the inelastic impact. Thus, for the $2p_1$ state, recoil energies of ~ 0.0006 eV are expected.

The spectral line shape to be expected when a definite recoil speed (corresponding to a given E_R) is

[23] Here we have used Paschen notation to designate the levels.
[24] J. Z. Klose, Astrophys. J. **141**, 814 (1965).
[25] The argument for spherical symmetry in the excited $2p_1$ state follows from its designation as 3^1S_0 in Shortley notation. In the same notation the ground state of neon is 2^1S_0.
[26] A. P. Stone, Proc. Phys. Soc. (London) **74**, 424 (1959).
[27] H. Nagaoka and T. Mishima, Sci. Papers Inst. Phys. Chem. Res. Tokyo **25**, 223 (1934).

superposed on the normal thermal motion has been shown to be[9]

$$I(\tilde{\nu})=(a/4b)[\mathrm{erf}(a\tilde{\nu}+b)-\mathrm{erf}(a\tilde{\nu}-b)], \qquad (4)$$

where $a=(Mc^2/2kT)^{1/2}/\tilde{\nu}_0$ and $b=(2E_R/kT)^{1/2}$, T being the gas temperature and $\tilde{\nu}_0$ the frequency (in wave numbers) at the center of the line. Equation (4) is normalized to unit area under the contour. This expression, together with the isotope shift and abundance data, has been used to generate the predicted contour shown in Fig. 4. It will be seen that at 300°K the observed half-width for the Ne_{20} component is 0.065 cm^{-1}, while the predicted value is 0.048 cm^{-1}. The additional width observed is evidently the result of a finite pressure-broadening contribution at 2.3 Torr, as discussed in the next subsection, and a small contribution of instrumental origin.[28]

C. Pressure Broadening

A pronounced increase in the width of the λ5852 discharge line is noted with increasing gas pressure, the line doubling in width as the pressure is increased from "0" to ~30 Torr at 300°K. This strong pressure broadening evidently results from the fact the lower state ($1s_2$) of the λ5852 transition is a resonance state which has a high radiative transition probability to the ground state and therefore interacts very strongly with the normal neon atoms.

The observed widths at half-maximum intensities, as measured with the etalon of finesse = 42, are shown in Fig. 5. The solid points have been obtained with the TE_{101} mode cavity containing the small quartz sphere and with the magnetron power set to give maximum intensity in the discharge. The fact that the extrapolation of these data to zero pressure leads to a width of 0.059 cm^{-1} instead of the expected 0.054 cm^{-1} for the 10-mm spacer[28] suggests that the high plasma density causes significant Stark broadening, and/or there is a sufficient density of resonance ($1s_2$) states that some self-absorption of the center of the line is taking place, leading to an increase in the measured width at the half-intensity points.

The excess broadening with increased discharge intensity has been investigated in more detail with the TE_{303} mode cavity and larger sphere. As seen from Fig. 5, an increase in the discharge λ5852 intensity by a factor of 10 produces a noticeable increase in linewidth, especially at low pressures. Therefore, the pressure broadening by collisions with neutral atoms is evaluated by ignoring the intense discharge points (open circles). The vertical lines attached to two of the solid dots in the figure represent an estimate of the possible systematic errors in the linewidth determination resulting from

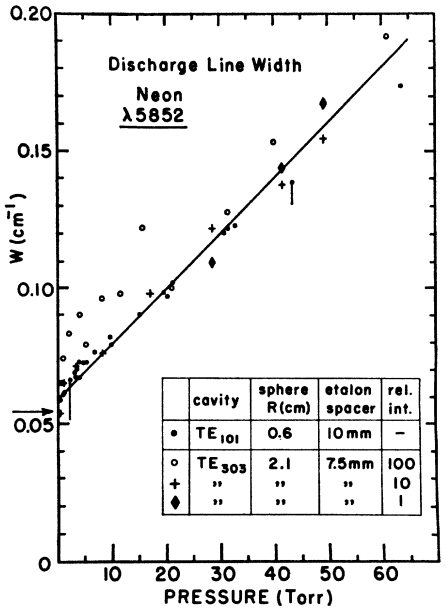

FIG. 5. Variation of the λ5852 discharge line width with gas pressure at 300°K for a variety of experimental conditions. The F-P plates of finesse 42 were used in these studies. (See text for discussion.)

instrumental and plasma broadening effects, while the reproducibility of a given half-width measurement involves a statistical error of approximately ±3%.

Although, as indicated by the solid line, an approximately linear increase in half-width with increasing neon gas pressure is observed over this limited pressure range, there is no reason to expect such a simple behavior, since the "core" of the line profile is determined in a rather complicated way by both Doppler and collision effects. Lang,[29] using photographic recording of Fabry-Perot patterns to determine pressure broadening of neon spectral lines, found a linear increase in the observed linewidths from 0 to ~300 Torr. The zero-pressure intercept showed a large instrumental contribution (~0.1 cm^{-1}) to his measurements. He expressed his results in terms of a pressure-broadening rate of ~0.012 cm^{-1}/Torr, which is approximately half the slope of the line shown in Fig. 5. As mentioned above, this method of expressing the results is invalid, since the actual rate of increase of half-width should be a complicated function of pressure in this range. The two measurements of the pressure dependence of the increase in half-width do agree in the sense that, at our highest pressure, ~60 Torr, our half-width determination of ~0.18 cm^{-1} is in essential agreement with Lang's value at the same pressure, when his data are corrected for his substantial instrumental width.

[28] The calculated instrumental width for plates of finesse 42 and 1-cm spacer is 0.012 cm^{-1}. From the analysis of R. Minkowski and H. Bruck, Z. Physik **95**, 299 (1935), which is strictly applicable only for Gaussian line shapes, a half-width of 0.054 cm^{-1} should be observed when the Doppler half-width is 0.048 cm^{-1}.

[29] K. Lang, Acta Phys. Austriaca **5**, 376 (1951). Although Lang assumed a negligible instrumental contribution to his observed widths, data presented by him at 300 and 77°K, together with the analysis of Minkowski and Bruck, (Ref. 28) suggest that his actual instrumental width was 0.097±0.002 cm^{-1}.

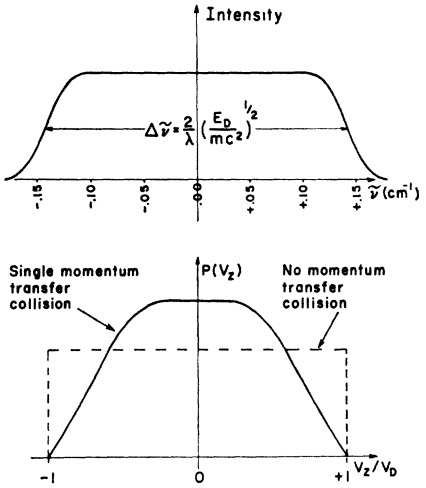

FIG. 6. Top: Predicted line shape at 300°K for λ5852 radiation emitted from excited atoms produced by dissociative recombination, with $E_D=1.3$ eV. Bottom: Probability, $P(v_z)$, of observing a particular z component of velocity in a group of atoms; (a) dissociatively produced with speed v_D (dashed line), and (b) following a single momentum-transfer collision (solid line). See text for discussion.

To the extent that these pressure-broadening determinations are free of plasma-broadening effects, they provide values for the width of the λ5852 line emitted by atoms moving with thermal velocities and therefore represent *minimum* values in the afterglow, no matter what the source of the radiation. We will make use of this point in some of the observations described in Sec. V.

D. Dissociative-Recombination Broadening and Collision-Narrowing Effects

If the dissociative-recombination process, Eq. (1) and Fig. 1, involves molecular ions in a particular initial state and moving with ambient thermal velocities, then the kinetic energy of dissociation superposed on the thermal motion leads to a Doppler-broadened line of the form given in Eq. (4), as Rogers and Biondi[9] have shown. In the dissociative case, $a=(Mc^2/kT)^{1/2}/\tilde{\nu}_0$ and $b=(E_D/kT)^{1/2}$. An example of the predicted line shape at $T=300$°K for a dissociation kinetic energy $E_D=1.3$ eV (see Fig. 1) is given in the upper half of Fig. 6. Here the small contribution to the line profile of the Ne_{22} isotope has been neglected. It will be noted that the width at half-intensity gives E_D directly, provided that $E_D \gg kT$, as is usually expected. In addition, the observation of such a characteristic flat-topped line shape should provide convincing evidence of the operation of a dissociative process in the formation of the excited state.

As discussed in Sec. III, the simple dissociative line shape will not be observed if the probability for the excited atom making either a momentum transfer or an excitation transfer collision is appreciable compared to the radiative probability. Obviously, one wishes to work at the lowest possible pressures to reduce these collision rates; however, pressures of $\gtrsim 1$ Torr were found necessary in our experiments in order to obtain reasonable plasma densities and light intensities and to avoid interfering effects (to be discussed shortly). Therefore, even at the lowest pressures used, excitation and/or momentum transfer effects could not be neglected.

The effect on the line shape of excitation transfer between excited (*) and normal atoms,

$$Ne_f^* + Ne_s \rightleftarrows Ne_f + Ne_s^*, \tag{5}$$

where the subscripts f and s refer to fast and slow atoms, respectively, is readily obtained. The slow-excited atom which is produced by such a reaction will radiate the thermal Doppler-plus-pressure broadened line of the type discussed in Sec. IV C and Fig. 5. Thus, if dissociative recombination and excitation transfer are the only significant processes, the λ5852 line consists of the broad, flat-topped dissociative profile representing those atoms which radiate before excitation transfer occurs, surmounted by a narrower core representing the atoms which have undergone excitation transfer.[30] As will be seen in Sec. V B, for this case it is possible to decompose the observed line profile into the contributions of fast and slow atoms to the intensity at each frequency and thus to evaluate the excitation-transfer cross section.

The effect on the simple dissociative line profile of momentum-transfer collisions, which slow the fast atoms, has been calculated.[31] The results are illustrated in the lower half of Fig. 6. In the simplest dissociative case, where there is a single dissociation speed, $v_D=(E_D/m)^{1/2}$,

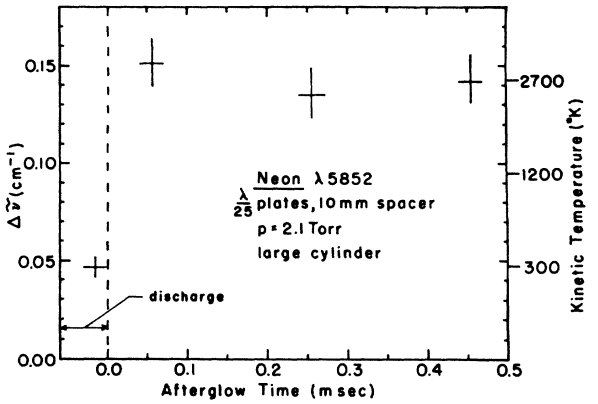

FIG. 7. Observed half-width of the λ5852 line during the discharge and the afterglow at 2.1 Torr and 300°K. The widths have been corrected for the substantial instrumental contribution arising from the use of Fabry-Perot plates of finesse ≃10. The scale at the right indicates the temperatures required if the widths are ascribed to thermal motion of the excited atoms.

[30] Since the excited-atom density is very small compared to the normal atom density, there is negligible probability that excitation transfer back to a fast atom will occur.

[31] T. R. Connor, M. S. thesis, University of Pittsburgh, 1964 (unpublished).

and thermal motion can be neglected, the probability of observing a particular component of velocity in the observer's (z) direction is uniform for $0 \leqslant |v_z| \leqslant v_D$, as indicated by the dashed line. Following one momentum-transfer collision between the excited atom and a normal neon atom, assuming isotropic scattering in the center-of-mass system, the uniform speed of dissociation, v_D, is degraded and the new velocity vectors have the z components indicated by the solid line. Since the intensity distribution in the emitted line, $I(\Delta\tilde{\nu} = \tilde{\nu}_0 v_z/c)$, is directly proportional to $P(v_z)$, one can see that the broad, flat-topped line of the type shown at the top of Fig. 6 will suffer increased rounding of its edges and a reduction in the width of the flat portion if momentum-transfer rates are not negligible compared to excitation-transfer and radiative-transition rates.

V. AFTERGLOW-RADIATION OBSERVATIONS

A. Linewidth Determinations

In the studies using the Fabry-Perot plates of finesse ~ 10, the substantial instrumental broadening of the $\lambda 5852$ line obscured details of the line shape of the sort discussed in Sec. IV D. Therefore, only a determination of the apparent linewidth at half-maximum intensity was attempted and the "actual" linewidth determined by correcting the observed half-width for instrumental broadening by the method of Minkowski and Bruck,[28] which strictly applies only to a Gaussian (e.g., thermal Doppler) line shape.

In these measurements we encountered difficulty at low pressures in obtaining sufficient $\lambda 5852$ intensity for adequate signal-to-noise level in the recordings of the afterglow line profiles. Observations with the small (radius = 0.6 cm) sphere in the TE_{101} cavity were therefore supplemented by observations in a large Pyrex cylinder (radius = 2.6 cm, length = 19 cm) enclosed in a high mode cylindrical cavity. In this case, the lower rate of plasma loss in the discharge and afterglow yielded higher afterglow intensities. (This cavity was, however, not suitable for electron-density determinations.)

The behavior of the linewidth in the discharge and during the afterglow at the lowest pressure (2.1 Torr) attained in this phase of the studies is shown in Fig. 7. The horizontal extent of the symbols indicates the time interval during which the photomultiplier was sensitive, while the vertical extent of the symbols indicates our estimate of the scatter in the determinations, together with possible systematic errors as a result of inadequacies in our correction for the instrumental broadening.[28] It will be seen that, during the discharge, the linewidth has approximately the thermal Doppler-plus-pressure-broadened value (~ 0.05 cm^{-1}) inferred from the studies with the F-P plates of finesse = 42. However, some 50 μsec later, in the afterglow, the linewidth has abruptly increased to several times the discharge value. In order for this to be a thermal effect, the excited-atom

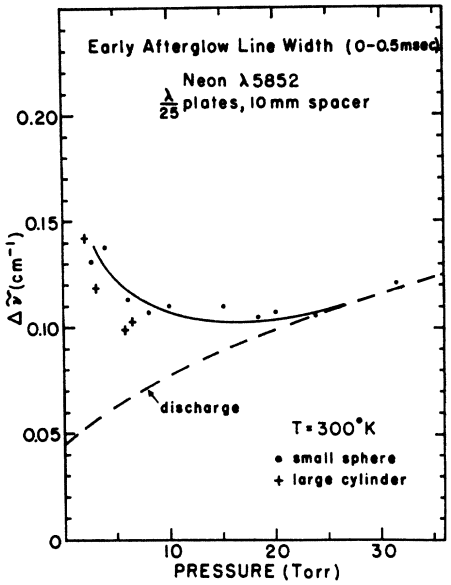

FIG. 8. Comparison of the early afterglow linewidth (0–0.5 msec) with that observed during the discharge as a function of neon gas pressure.

temperature would have to abruptly increase to ~ 2800°K, as indicated by the scale at the right of the figure.

A more reasonable explanation of the abrupt broadening is that the afterglow radiation results from dissociative recombination, and conditions at this pressure are such that a substantial fraction of the fast-excited atoms radiate before transferring excitation to slow-normal atoms. If this is the case, an increase in neon pressure should result in a narrowing of the line as a result of the larger fraction of excitation transfers before radiation.

The data obtained with the small sphere and the large cylinder are shown in Fig. 8. For clarity, the discharge data points and the error bars have been omitted from the figure. The discharge data scatter less than $\pm 10\%$ about the dashed curve. It will be seen that the expected narrowing of the early afterglow line occurs with increasing pressure (in these studies there is insufficient intensity to obtain linewidths later in the afterglow than 0.5 msec). Also, the afterglow line does not become narrower than the discharge line. As noted in Sec. IV C, such a result is to be expected if the discharge linewidth is principally determined by thermal Doppler and pressure-broadening effects. In the afterglow the thermal-excited atoms produced by excitation (or momentum) transfer from the initially fast-excited atoms should radiate a similar line.

From the rate of decrease of linewidth with increasing pressure one can estimate that the excitation transfer cross section must be of the order of 10^{-15} cm^2 to produce such an effect. A more quantitative determination of the excitation transfer is given in the analysis of the line shape studies in Sec. V B.4.

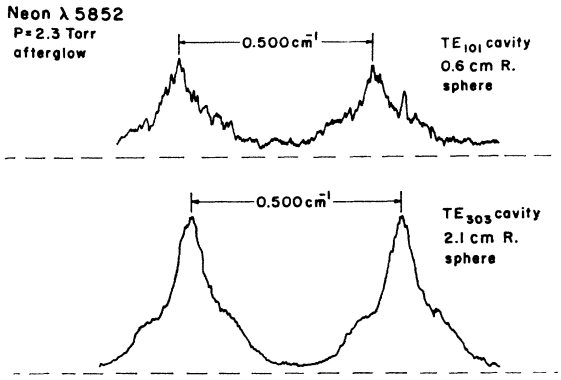

FIG. 9. Tracings of the chart records of the afterglow λ5852 line profiles at 300°K, showing the improved signal-to-noise ratio obtained with the larger sphere. Only two of the interference orders traced are shown in each case, although as many as 14 others are sometimes recorded. The dashed lines indicate the dark current level in each case.

B. Line-Shape Studies

1. Observed Line Profiles

The linewidth determinations described in the preceding subsection agree in all respects with a dissociative recombination origin of the afterglow radiation; however, accurate determinations of the line *shapes* should provide additional evidence, since a rather characteristic line shape is predicted for the dissociative case. We, therefore, obtained improved Fabry-Perot plates of finesse ~42 at λ5852, resulting in sufficiently small instrumental broadening to permit reasonably accurate determinations of the spectral line profiles.

As in the earlier studies, it is difficult to obtain sufficient afterglow intensity with the small sphere to permit accurate line-shape determinations at afterglow times of $\gtrsim 1$ msec. Thus, a larger sphere (2.1 cm radius) within a TE_{303} mode cavity has been used for many of the studies. An example of the resulting improvement in signal-to-noise ratio obtained in the later afterglow (>1 msec) is shown in Fig. 9, which is a tracing of the chart records of the line profiles. It should be noted that, as a result of the redundancy in information obtained in tracing through a number of interference orders of the Fabry-Perot pattern, it is possible to average out much of the noise evident in the traces by successively overlaying the several orders and obtaining the mean value of the curves. Thus, even the average curve of the upper trace of the figure clearly shows a pronounced broadening relative to the discharge line (compare with Fig. 4).

Examination of curves obtained by averaging several orders of chart records of the type shown in the lower half of Fig. 9 indicates that the line profile evidently consists of a relatively narrow core on top of a rather broad base, as expected if dissociative recombination and excitation transfer are the important processes in determining the line shape. In fact, as we shall see shortly, the central core has the thermal-plus-pressure broadened shape of the discharge line.

2. Interfering Line Effects

In attempting to work at as low a pressure as possible to reduce the excitation-transfer-produced core of the line relative to the broad base, it was discovered that other neon lines, such as λ5811 ($4d_2-2p_8$) and λ5764 ($4d_4'-2p_9$), were leaking through the λ5852 interference filter. Fortunately, such unwanted lines change their positions relative to the desired line as the order is changed, so that they can be detected by their movement. In fact, the λ5811 and λ5764 radiations in the F-P profiles have been identified by their rate of movement relative to λ5852.

Although grating spectrometer studies of the relative intensities of the various lines as a function of time in the afterglow suggest that unwanted lines are a serious problem in the line-shape determinations only at low (<1 Torr) pressures, an additional check on the reality of the broad "shoulders" on the λ5852 line has been made by taking line profiles with different etalon spacers. Typical results, using a 12.5 mm and a 7.5-mm spacer instead of the 10-mm spacer, are shown in Fig. 10, which presents tracings of the chart records. It will be seen that, in spite of substantial changes in the free spectral ranges (which have the effect of displacing even close-lying unwanted lines) the "shoulders" in the curves are evident even on the unaveraged tracings.

3. Analysis of the Line Shapes

The large number of line-shape tracings obtained at various afterglow times and neon gas pressures support the conclusion that the line shape is principally determined by dissociation and excitation transfer. Thus, the line can be decomposed into a fast atom (radiation before excitation transfer) and a slow atom (radiation after excitation transfer) component. Two methods

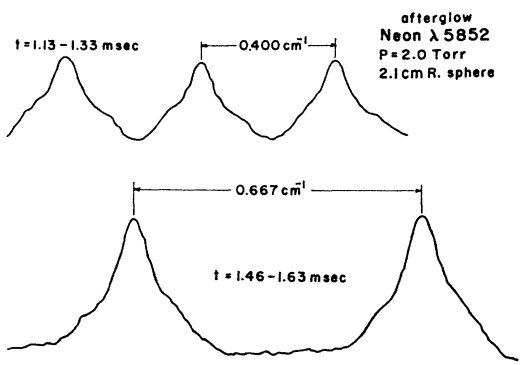

FIG. 10. Tracings of the chart records of the afterglow λ5852 line profiles obtained with two different etalon spacers, indicating that the "shoulders" on the line profile are not the result of other interfering spectral lines.

have been used to accomplish this decomposition, each method yielding quite similar results. In both cases we start with a line profile obtained by averaging the tracings over several interference orders. An example of the results of this averaging is shown in Fig. 11, which represents the mean curve obtained from several interference orders in the record shown in the lower half of Fig. 10.

In the first method, the discharge line profile, which is also recorded in most runs, is scaled to fit the afterglow profile so that its upper portions coincide with the core of the afterglow line. The scaled line shape is indicated by the dashed and solid curve marked "slow" in Fig. 11. The fast-atom contribution is then obtained by subtracting this "slow" profile from the solid line. The remainder, indicated by the solid and dashed line marked "fast," is seen to be rather broad and somewhat flat topped. The slight asymmetry in the fast component evidently is the result of a small contribution of another spectral line leaking through the filter.

The second method of decomposing the afterglow line into a fast and a slow component is to note the position of the "shoulders" on the averaged profile (especially on the low-frequency side, which is free of the isotope shift distortion of the central core) and to draw a horizontal line at this value of the intensity in order to separate the fast and slow components. In this case, one can compare the half-width of the slow component with the discharge width, since we have not forced the two to be equal, as was done in the first method. Comparison of the two methods applied to the same line profiles indicates that, within $\sim 10\%$, there is agreement concerning the half-widths and intensities ascribed to the slow and to the fast components.

Having divided the line profile into a fast and a slow atom component, the widths at half-intensity should reflect the dissociation kinetic energy and the Doppler-plus-pressure broadening contributions, respectively. In the case shown in Fig. 11, $W_f = 0.27$ cm^{-1} corresponds to a dissociation kinetic energy of $E_D \sim 1.2$ eV. The inferred line profile is, however, somewhat more rounded than

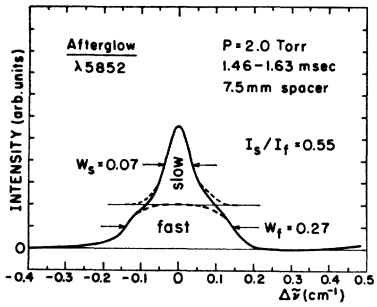

FIG. 11. Observed afterglow line profile at 300°K obtained by averaging data obtained from several interference orders. The decomposition of the line profile into a "fast-" and a "slow-" atom component is indicated in the figure, while the details of the methods used are given in the text.

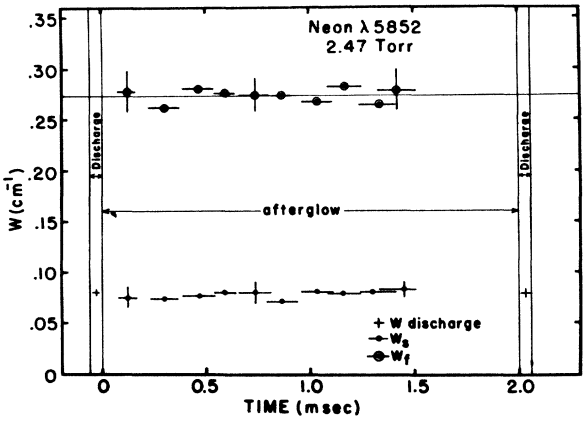

FIG. 12. Observed widths of the fast- and slow-atom components of the λ5852 line profile as a function of time at 300°K.

the simple dissociative case treated in Sec. IV D.1 and Fig. 6.

If the analysis presented is valid, then W_f and W_s, the half-widths of the fast- and slow-atom components, respectively, should be independent of time in the afterglow, and W_f should *not* decrease with increasing neon pressure. The first point is illustrated in Fig. 12, which shows the linewidths observed with the large sphere in the discharge and during the afterglow at a pressure of 2.47 Torr. The horizontal extent of each symbol indicates the time gate of the measurement; the several vertical lines indicate estimated random and systematic probable errors. Within the accuracy of the determinations the value of W_s is constant during the afterglow and equal to $W_{\text{discharge}}$. The fast component of the afterglow line is found to maintain a half-width $W_f \simeq 0.27$ cm^{-1} throughout the period studied, 100 μsec to 1.5 msec.

The dependences of W_f and W_s on the neon pressure are shown in Fig. 13, which presents data obtained both with the large and the small spheres. While the large- (2.1-cm-radius) sphere data represent average values for 0.1–1.5 msec of the afterglow, the data for the small (0.6 cm radius) sphere refer only to the earlier afterglow times $\gtrsim 0.5$ msec, where sufficient intensity was available for the measurements. Again, because of intensity problems, data at the lowest pressures could only be obtained with the larger sphere. The observed lack of dependence of W_f on pressure confirms our assumption that simple dissociation and excitation transfer determine the recombination line shape, with such effects as momentum transfer collisions of the excited atoms of lesser importance.

4. *Excitation Transfer Determination*

If a rather simple model is assumed to describe the origin of the afterglow radiation, it is possible to obtain from the observed line profiles a measure of the excitation-transfer cross section for reaction (5). Let us

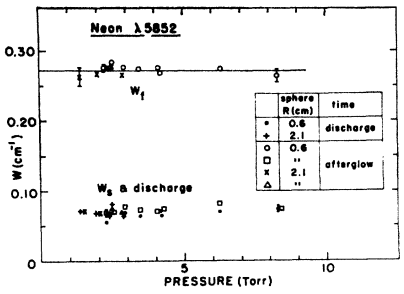

FIG. 13. Observed widths of the fast- and slow-atom components of the λ5852 line profile as a function of neon gas pressure as measured in the two spheres at 300°K.

suppose that, over most of the pressure range studied, the dissociative recombination reaction is responsible for the production of the excited atoms in the afterglow. Reference to Fig. 1 indicates that the $2p_1$ state is only one of a number of possible excited states produced in this manner.[32] We shall assume that there is a fixed probability per recombination of producing each of the excited states.

Thus, the upper state of the observed λ5852 ($2p_1-1s_2$) transition is populated both directly by recombination and by cascading from higher states produced by recombination. Since the cascading states are principally in dipole interaction with the ground state, we shall assume that the fast-excited atoms in these states have a large probability of undergoing excitation transfer before radiating; thus, cascading contributions to the $2p_1$ state will be assumed to involve thermal velocity excited atoms. We have been unable to evaluate this cascading contribution to the population of the $2p_1$ state, since the most important transitions lie in the infrared, beyond the range of our photomultiplier detectors.

The directly produced, fast-$2p_1$ excited atoms are assumed to have an appreciable probability for excitation transfer to slow atoms before radiating. If we denote the density of excited $2p_1$ atoms by X, the fast (dissociatively produced) group obeys the equation

$$\partial X_f/\partial t = P_{\rm dir} - \nu_r X_f - \nu_x X_f, \tag{6}$$

where the production of this state, $P_{\rm dir}$, is the rate of dissociative recombination directly to the $2p_1$ state, ν_r is the reciprocal of the radiative lifetime of the $2p_1$ state, and $\nu_x = nQ_x v$ is the excitation transfer frequency at the relative velocity v between the fast-excited atom and the slow normal atom, n being the neon gas density and Q_x the excitation transfer cross section.

The slow-excited atoms result from cascading and from excitation transfer. Since cascading times are short compared to the time scale of our measurements ($\gtrsim 100$ μsec), the rate of change of density of the slow component may be written as

$$\partial X_s/\partial t = P_{\rm cas} + \nu_x X_f - \nu_r X_s, \tag{7}$$

where $P_{\rm cas}$ represents the rate of dissociative recombination into the various higher states that cascade into the $2p_1$ state. Since, in both equations, $\partial X/\partial t$ can be shown to be small compared to each of the terms on the right of the equations, we have

$$X_f \simeq P_{\rm dir}/(\nu_r+\nu_x) \tag{8}$$

and

$$X_s \simeq (\nu_x/\nu_r)[P_{\rm dir}/(\nu_r+\nu_x)] + P_{\rm cas}/\nu_r. \tag{9}$$

The fast and slow contributions to the line intensity, I_f and I_s, are proportional to the densities of fast and slow excited atoms; thus,

$$I_s/I_f = X_s/X_f \simeq (\nu_x/\nu_r)(1+P_{\rm cas}/P_{\rm dir}) + P_{\rm cas}/P_{\rm dir}. \tag{10}$$

A linear increase with neon gas density is predicted for the ratio I_s/I_f, the intercept giving the ratio of cascading to direct production of the $2p_1$ state by recombination and the slope a measure of the excitation transfer cross section.

Analysis at various pressures of the line profiles of the type illustrated in Fig. 11 yields the required I_s/I_f ratios. There are large uncertainties in these deduced values, as evidenced by random variations in the ratios obtained at later afterglow times. In addition, at low pressures in the larger sphere, the ratio I_s/I_f is somewhat larger than its final value early in the afterglow ($\lesssim 500$ μsec), as indicated in Fig. 14. This effect may result from some direct excitation of the $2p_1$ state by "hot" electrons left over from the discharge, since the electron energy decay time ($\sim M/2m\nu_c$, where ν_c is the electron elastic collision frequency) is the order of 200 μsec at 1 Torr. In any event, ratios of I_s/I_f are only given if measurements could be made for a long enough afterglow period to reach a constant value at each pressure.

The variation in the deduced I_s/I_f values with pressure is shown in Fig. 15. The several vertical bars again indicate our estimate of possible systematic errors in the determinations, the random errors being somewhat smaller. Only the larger sphere provided sufficient intensities to reach late enough afterglow times for constant I_s/I_f values at the lower pressures. In accordance with the prediction of Eq. (10), we have drawn

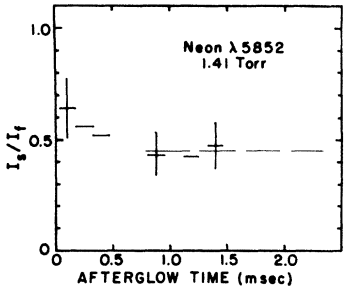

FIG. 14. Observed variation of the ratio of intensities in the slow- and fast-atom components of the λ5852 line profile as a function of time in the afterglow at 300°K.

[32] Starting with a molecular ion in a particular state (e.g., the ground-vibrational state of the electronic state shown in the figure) any excited state for which $E_D>0$ may be formed by dissociative recombination, providing the necessary curve crossings occur.

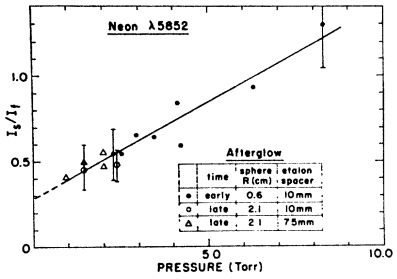

FIG. 15. Variation in the deduced ratios I_e/I_f with neon gas pressure at 300°K for a variety of experimental conditions.

the best straight line through the data, although the accuracy of the data by no means suggests that this is a unique fit. From the analysis, the excitation transfer cross section for excited atoms of speed 2.5×10^5 cm/sec is found to be $Q_x=(8\pm2)\times10^{-16}$ cm^2.

C. Correlations of Line Intensities and Electron Densities

In the course of the measurements of the line shapes, periodic checks have been made with the grating monochromator, using a gated 931A photomultiplier as detector, in order to monitor the presence of other afterglow lines which might interfere with the shape determinations. At the same time the microwave apparatus has been used to measure average electron densities. Thus, it is possible to compare the rates of decay of the various spectral line intensities with that of the electron density over most (0.2–1.8 msec) of the afterglow period.

During this limited observation interval, the line intensities decrease only by a factor of ~10; this is too small a range to establish accurate correlations of line intensity and electron density. Nevertheless, the intensity decays have been compared with the variation of n_e^2 (a linear proportionality is expected if the radiating state is produced at the rate $\alpha_j n_e[Ne_2^+]$ and if $n_e\simeq[Ne_2^+]$, α_j being the two-body recombination coefficient into the particular radiating state[33]). The observations at $p\sim1$ Torr, for example, indicate that the intensity of λ5852 ($2p_1$-$1s_2$) varies approximately as n_e^2, though slightly slower, that of λ5945 ($2p_4$-$1s_5$) varies as n_e^2, as do λ6030 ($2p_2$-$1s_4$) and λ6402 ($2p_9$-$1s_5$) while λ5764 ($4d'_4$-$2p_9$) decreases somewhat more rapidly than n_e^2, but more slowly than n_e^3, as do λ5811 ($4d_2$-$2p_8$), λ6334 ($2p_8$-$1s_5$), λ6507 ($2p_8-1s_4$), λ6599 ($2p_2$-$1s_2$) and λ6678 ($2p_4$-$1s_2$). At $p=2.5$ Torr, similar behavior (variation as $\sim n_e^2$) is again noted for λ5852, λ6030, and λ6402, while λ6334 and λ6678 decrease slightly faster in intensity than n_e^2. These limited range comparisons are consistent with the hypothesis that much of the afterglow radiation originates from two-body electron-ion recombination; however, the short afterglow periods resulting from the required high repetition rate are not sufficient to insure that ion production and conversion reactions in the afterglow have diminished to negligible proportions.

An order of magnitude estimate of the absolute intensities of λ5852, obtained by consideration of the transmission of the various optical elements, the aperture of the optical apparatus, the published sensitivity of the photomultiplier, etc., together with the measured average electron densities, yields a value, $\alpha_j\sim3\times10^{-9}$ cm^3/sec, for recombination into the $2p_1$ excited state. Since λ5852 is but one of more than 10 strong afterglow lines which represent independent (i.e., not cascading) transitions, it appears that the over-all recombination coefficient deduced from the absolute intensity estimate exceeds 3×10^{-8} cm^3/sec. This yield is at least an order of magnitude greater than that expected from collisional-radiative recombination of Ne^+ ions and electrons, even assuming $[Ne^+]\simeq n_e$.

VI. DISCUSSION AND CONCLUSIONS

Our investigation of the nature of the electron-ion recombination process in neon has centered mainly on studies of the linewidth and details of the line shape of the λ5852 ($2p_1$-$1s_2$) transition. In addition, our electron density decay studies indicate that, even at electron densities in the 10^{10}-10^{11} cm^{-3} range, two-body capture with a coefficient $\alpha\simeq2\times10^{-7}$ cm^3/sec is still predominant, so that collisional-radiative[1] and the recently proposed collisional-dissociative[34] processes, which are three-body in character, are of substantially less importance. (At 300°K and $n_e\sim3\times10^{10}$ cm^{-3}, the effective coefficients for these processes are predicted to be $\alpha_{c.r.}\sim3\times10^{-9}$ cm^3/sec[10] and $\alpha_{c.d.}\sim1\times10^{-8}$ cm^3/sec[34].)

In the linewidth studies (carried out with the medium finesse Fabry-Perot plates having appreciable instrumental broadening) the width at half-intensity of the observed profiles is found to increase markedly in going from the discharge (electron impact excitation of the neon $2p_1$ radiating state) to the afterglow (population of the $2p_1$ state by recombination). Further, the afterglow linewidth decreases with increasing gas pressure. Both observations are consistent with production of fast-$2p_1$ excited neon atoms in the afterglow by the dissociation of Ne_2^+ ions on capturing electrons. The decrease in linewidth with increasing pressure evidently results from the increasing likelihood of transfer of excitation from the fast-excited atoms to the slow-normal atoms before radiation can occur.

[33] The stated relationship between intensity and electron density applies to a microscopic volume element. The microwave apparatus provides an average of the electron density over the container volume which is quite different from the average radiant intensity "seen" by the optical apparatus. E. Zipf (private communication), has shown that substantial deviations from the microscopic relationships between I and n_e can occur for the volume-averaged quantities when the electrons and ions are not distributed uniformly throughout the ionized gas. However, the various afterglow line intensities should all be affected in like manner.

[34] C. B. Bollins, Phys. Rev. (to be published).

More definitive results have been obtained from the line-shape studies achieved with the high finesse F-P plates, in which instrumental broadening effects are small. Here, by averaging data over a number of interference orders of the F-P etalon, we have been able to obtain afterglow line shapes (see Figs. 9–11) which exhibit essentially a thermal atom "core" atop a broad, rather flat-topped pedestal of the form expected if the radiating atoms are dissociatively produced with a speed substantially in excess of thermal speeds.

The observed shape, e.g., Fig. 11, falls somewhat more slowly in the wings of the line than theoretically predicted for excited atoms produced by dissociation of molecular ions in a single electronic or vibrational state (see Fig. 6). This added rounding of the wings of the profile may result from the fact that the cross section for momentum transfer collisions is almost as large as the excitation transfer cross section. Indeed, if the analysis leading to the value $Q_x \sim 8\times10^{-16}$ cm^2 is correct,[35] it is difficult to see how the momentum transfer cross section for the $2p_1$ atoms can be very much smaller.

Two observations support the supposition that the momentum transfer cross section is, in fact, smaller than the excitation transfer cross section. Over the pressure range studied, the line profiles exhibit the "shoulders" characteristic of a mixture of fast- and slow-atom radiation, rather than the smoothly broadened shape expected if slowing collisions outweigh excitation transfer to thermal atoms. In addition, the deduced values of the fast-component half-width do *not* decrease with increasing pressure as expected if slowing collisions occur more often than excitation transfer collisions.

A second possible explanation of the added rounding in the wings of the line is that the $2p_1$ atoms are produced from molecular ions in more than one vibrational or electronic state, leading to more than one value of E_D. With the present signal-to-noise ratios in the line profile records, we can not hope to see the weak additional "shoulders" in the profile that would be expected from this effect, only a smoothed additional broadening.[36]

Returning to the main features of the line profiles, on the assumption that a single molecular ion state contributes principally to the production of the $2p_1$ state, we obtain from W_f, the half-width of the fast component, a value for the kinetic energy of dissociation of the fragments, $E_D \simeq 1.2$ eV. If the potential energy curves were indeed as simple as is indicated in Fig. 1, we could now determine $D(Ne_2^+)$, the dissociation energy of the molecular ion in the single electronic state shown. However, the schematic potential curves of Fig. 1 are oversimplified in a number of respects. For one, we have shown the ionization potential of Ne^+ as 21.6 eV, which corresponds to the lower of the two possible ground-state ionic configurations ($2P^0_{3/2}$). The other configuration ($2P^0_{1/2}$) lies 21.7 eV above the ground state. Second, we have shown only one attractive branch of the Ne_2^+ potential curve and only one repulsive branch of the unstable excited molecule, while there are several for each. If we assume that λ5852 radiation is produced by recombination of Ne_2^+ ions in their ground-vibrational state, then, from the known position of the $2p_1$ energy level, together with the deduced E_D value, we conclude that $D(Ne_2^+) \simeq 1.4$ or 1.5 eV, depending on which molecular-ion state exhibits the necessary curve crossing with the repulsive curve leading to the $2p_1$ state.

A value of $D(Ne_2^+)$ of $\sim$1.4 eV raises the question of how λ5764 and λ5811, which originate from levels $\sim$0.85 eV below their ionization limit, can be important afterglow recombination lines. We have ruled out collisional-radiative recombination, which can directly produce the required excited states, on the ground that its recombination rate is orders of magnitude too small. Dissociative recombination can produce the required excited states if the molecular ions are not all in their lowest vibrational or electronic states. While studies of molecular spectra in helium afterglows provide some indirect evidence that vibrational excitation of He_2^+ relaxes in <1 msec,[11] spectral line-broadening studies in helium[9] appear to require the presence of molecular ions in a state well above the $v=0$ vibrational level of the A state during the afterglow. Thus, persistence of vibration in Ne_2^+ at low pressures may account for the presence of the λ5764 and λ5811 lines. Alternatively, the other electronic configurations of the Ne_2^+ ion may exhibit smaller dissociation energies than $D \simeq 1.4$ eV making it energetically possible to reach the upper excited states of the λ5764 and λ5811 transitions. If the necessary curve crossings between molecular ion and unstable excited molecular states occur, the lines will then be a part of the recombination radiation.

Our success in observing a line profile exhibiting the characteristic "broad-shouldered" profile of the dissociative recombination process hinged on the occurrence of a sufficiently small excitation transfer cross section ($\lesssim 10^{-15}$ cm^2) between the fast-excited atoms and the thermal normal atoms. The analysis presented in Sec. V B.4, although subject to considerable uncertainty, is consistent with an excitation transfer cross section of $\sim 8\text{-}13\times10^{-16}$ cm^2. Since cross sections very much larger are sometimes encountered in excitation transfer processes, it appears that the required weak interaction between the $2p_1$ excited atoms and the normal atoms results from the spherical symmetry of the atomic states in each case. However, we lack accurate wave functions for the excited state; thus, this explanation must be regarded as speculative.

Although the present study of recombination in neon afterglows presents strong evidence for the predomi-

[35] In the analysis presented in Sec. VB4., if cascading production of the $2p_1$ atoms is absent, the excitation transfer cross section deduced from the data is increased to $\sim 1.3\times10^{-15}$ cm^2.

[36] This point is being studied in an extension of this work by L. Frommhold and M. A. Biondi, involving considerably improved signal-to-noise ratios in the line profiles.

nance of two-body dissociative recombination, a recent summary by Ferguson *et al.*,[12] of experiments in helium indicates that many of the observations there are consistent with the predominance of three-body collisional-radiative recombination of electrons with He^+ and He_2^+ ions. However, two observations in helium indicate that recombination processes in addition to collisional-radiative recombination must also occur. Rogers and Biondi[9] observe that the helium afterglow line λ5876 exhibits broadening in excess of the discharge linewidth, an observation corroborated by Ferguson *et al.*[12] It is shown that, since effects such as plasma and pressure broadening can be ruled out, dissociative recombination is the likely source of the broadened afterglow line.

Further, on the assumption that both collisional-radiative ($He^+ + 2e$) and some dissociative ($He_2^+ + e$) recombination occur in helium, the observation that the λ5876 line exhibits less broadening at 77°K than at 300°K becomes plausible. Collisional radiative recombination yields thermal velocity excited atoms; therefore, since its rate increases more rapidly with decreasing temperature than does that of dissociative recombination, the afterglow line at 77°K has a larger fraction of slow atom component and appears narrower.

The second observation in helium which indicates that collisional-radiative is not the only recombination process which is important is the finding by Kerr and co-workers[13] that the afterglow molecular radiation at higher pressures (>15 Torr) strictly follows the square of the electron density over a wide range. Thus, a two-body recombination process, with coefficient in excess of 3×10^{-10} cm³/sec, is inferred. The two-body radiative limit of collisional-radiative recombination is orders of magnitude smaller; therefore, we can only conclude that the precise nature of the recombination processes in helium is, at present, not at all clear.

A final point, raised by Ferguson *et al.*,[12] concerns the applicability to ionospheric analyses of laboratory determinations of electron-ion recombination coefficients. They assert that we must critically reexamine the question of whether recombination rates determined at electron densities in the 10^9–10^{11} cm^{-3} range can be safely extrapolated for use under ionospheric conditions ($n_e \sim 10^4$–10^6 cm^{-3}) as a result of the occurrence of collisional-dissociative as well as dissociative recombination.

Collisional-dissociative recombination involves the capture of an electron by a molecular ion following energy exchange between that electron and another electron in the plasma. In this case the excited state of the molecule, lying below the molecular-ion state, is considered to be unstable, so that dissociation of the molecule lowers the excitation energy (by increasing the kinetic energy of the fragments) to the point where ionization of the excited atom by plasma electrons is unlikely.

Recent calculations by Collins[34] support two reasons for discounting the likelihood of interference by collisional-dissociative recombination in the laboratory determinations of ionospheric coefficients. First of all, the collisional-dissociative process is three-body (one ion, two electrons) in character, rather than two body (one ion, one electron) as is dissociative recombination, leading to a markedly different form of electron-density decay in the afterglow. Second, the effective coefficient at $n_e \sim 10^9$ cm^{-3}, where coefficients for ionospheric ions have been determined in the laboratory studies,[37] is $<10^{-9}$ cm³/sec for collisional-dissociative recombination, as opposed to the observed values of $>10^{-7}$ cm³/sec for N_2^+ and O_2^+ ions.[37]

Thus, the present studies of neon, in which the excited atoms are evidently produced by a dissociative process which exhibits a recombination coefficient of 2×10^{-7} cm³/sec at 300°K, strongly suggest that the similar coefficients for N_2^+ and O_2^+ ions and electrons are also the result of two-body dissociative recombination.

ACKNOWLEDGMENTS

We wish to thank our colleagues, especially L. Frommhold, T. Holstein, T. M. Donahue, and E. Zipf, for stimulating discussions and suggestions during the course of this work.

[37] W. H. Kasner and M. A. Biondi, see Ref. 8.